Nanoscale

PAPER

View Article Online
View Journal | View Issue

Cite this: *Nanoscale*, 2016, **8**, 14565

Gold core@silver semishell Janus nanoparticles prepared by interfacial etching†

Limei Chen, Christopher P. Deming, Yi Peng, Peiguang Hu, Jake Stofan and Shaowei Chen*

Received 25th April 2016,
Accepted 4th July 2016

DOI: 10.1039/c6nr03368g

www.rsc.org/nanoscale

Gold core@silver semishell Janus nanoparticles were prepared by chemical etching of Au@Ag core–shell nanoparticles at the air/water interface. Au@Ag core–shell nanoparticles were synthesized by chemical deposition of a silver shell onto gold seed colloids followed by the self-assembly of 1-dodecanethiol onto the nanoparticle surface. The nanoparticles then formed a monolayer on the water surface of a Langmuir–Blodgett trough, and part of the silver shell was selectively etched away by the mixture of hydrogen peroxide and ammonia in the water subphase, where the etching was limited to the side of the nanoparticles that was in direct contact with water. The resulting Janus nanoparticles exhibited an asymmetrical distribution of silver on the surface of the gold cores, as manifested in transmission electron microscopy, UV-vis absorption, and X-ray photoelectron spectroscopy measurements. Interestingly, the Au@Ag semishell Janus nanoparticles exhibited enhanced electrocatalytic activity in oxygen reduction reactions, as compared to their Au@Ag and Ag@Au core–shell counterparts, likely due to a synergistic effect between the gold cores and silver semishells that optimized oxygen binding to the nanoparticle surface.

Introduction

Transition-metal nanoparticles have been attracting significant attention in diverse research fields, such as (bio)chemical sensing, multifunctional catalysis, and drug delivery, primarily because of their rich chemical functionality.[1–5] These nanoparticles are generally formed with a symmetrical shape and composition because of minimization of surface energy; yet, in the quest for "smart" materials that may be exploited for directional engineering and functionalization, structurally asymmetrical Janus nanoparticles have emerged as a unique, new member of the family of functional nanomaterials.[6–10] For instance, Janus nanoparticles have been prepared based on metal–metal oxide heterodimer composites such as Au–SiO_2, Au–TiO_2 and Au–Fe_3O_4 nanoparticles.[11–13] Of these, Au–TiO_2 snowman-like Janus nanoparticles have been fabricated by directional growth of TiO_2 nanoparticles on gold Janus nanoparticles where one hemisphere is capped with hydrophilic ligands and the other hydrophobic, and the resulting heterodimers show apparent photocatalytic activity towards methanol oxidation to formaldehyde, due to enhanced charge separation of TiO_2 under photoirradiation by the gold nanoparticles, as compared to TiO_2 colloids alone.[12] Bimetallic Janus nanoparticles have also been prepared by asymmetric deposition of a second metal onto the surface of the core materials, forming a dumb bell or acorn-like structure, or by asymmetrical etching of the shell metal, forming metal-tipped nanorods.[14–16] For instance, dumbbell-like Ag-tipped Au nanorods have been prepared by lateral etching of core–shell Au@Ag nanorods and have shown improved catalytic activity for the reduction of *p*-nitrophenol due to their specific structure and ligand effect, as compared to the original nanorods.[15] Another method is based on galvanic exchange reactions whereby partial replacement of the original core metal with a second metal is carried out under strict spatial control.[17,18] In another study, AgPd and AuPd dimer nanostructures are prepared by kinetically controlled nucleation and growth of Ag or Au on only one facet of cubic Pd nanocrystals by manipulation of various parameters such as injection rate and capping ligands.[19] Such bimetallic structures endow the nanoparticles with unique optical and electronic properties, as well as electrocatalytic activity towards, for instance, the oxygen reduction reaction (ORR), a critical reaction in fuel cell electrochemistry, as compared to their monometallic counterparts.[20,21] In fact, in a previous study,[18] we prepared bimetallic AgAu Janus nanoparticles by galvanic exchange reactions of silver nanoparticles with a gold(I)–thiolate complex at the air/water interface, and the obtained Janus nanoparticles exhibited higher ORR activity than the original Ag nanoparticles, due to polarized distributions of electrons within the nanoparticles as a result of partial charge transfer from Ag to Au,

Department of Chemistry and Biochemistry, University of California, 1156 High Street, Santa Cruz, California 95064, USA. E-mail: Shaowei@ucsc.edu

† Electronic supplementary information (ESI) available: Additional TEM, UV-vis, XPS, and electrochemical data. See DOI: 10.1039/c6nr03368g

although the Au content was only 5 at%. In such bimetallic nanoparticles, additional contributions to enhanced ORR activity may arise from surface strain that facilitate oxygen adsorption onto the shell metal.[5,22] More complicated trimetallic Neapolitan nanoparticles have also been prepared by two sequential interfacial galvanic exchange reactions.[23]

In the present study, using Au@Ag core–shell nanoparticles as the starting materials, we prepared Au@Ag semishell Janus nanoparticles by selective chemical etching of part of the silver shell. The Au@Ag core–shell nanoparticles were produced by growing a silver shell onto gold seed nanoparticles and capping by 1-dodecanethiol. When a nanoparticle monolayer was formed on the water surface of a Langmuir–Blodgett trough, a mixture of H_2O_2 and NH_3 was injected to the water subphase to selectively etch off the bottom half of the silver shells, leading to the formation of Au@Ag semishell Janus nanoparticles. The asymmetrical structure of the resulting nanoparticles was characterized by a variety of microscopy and spectroscopy measurements. Interestingly, the semishell Janus nanoparticles exhibited enhanced electrocatalytic activity in ORR, as compared with the original core–shell nanoparticles, suggesting that interfacial engineering provided an effective way to manipulate and optimize the nanoparticle electronic properties and hence catalytic performance.

Experimental section

Chemicals

Hydrogen tetrachloroauric acid ($HAuCl_4{\cdot}xH_2O$) was synthesized by dissolving ultrahigh-purity gold (99.999%, Johnson Matthey) in freshly prepared aqua regia followed by crystallization. Silver nitrate ($AgNO_3$, Fisher Scientific), sodium borohydride ($NaBH_4$, ≥98%, Acros), sodium citrate dihydrate ($Na_3C_6H_5O_7{\cdot}2H_2O$, Fisher Scientific), sodium hydroxide anhydrous (NaOH, Fisher Scientific), L-ascorbic acid (ACS grade, Amresco), hydrogen peroxide (H_2O_2, 30% solution, Fisher Scientific), strong ammonia solution (NH_3, Fisher Scientific), 1-dodecanethiol ($CH_3(CH_2)_{11}SH$, 96%, Acros), and acetic acid (HOAc, Glacial, Fisher Scientific) were all used as received without any further purification. Solvents were purchased at the highest purity available from typical commercial sources and also used as received. Water was supplied by a Barnstead Nanopure water system (18.3 MΩ cm).

Synthesis of Au@Ag core–shell nanoparticles

In a typical synthesis, citrate-stabilized gold colloids of *ca.* 5 nm in diameter were prepared and used as the seed nanoparticles.[24] Experimentally, 0.05 mmol of $HAuCl_4$ and 0.05 mmol of sodium citrate were dissolved into 100 mL of H_2O at room temperature under magnetic stirring, into which was added dropwise 5 mL of an ice-cold, freshly made solution of 100 mM $NaBH_4$. The appearance of a dark red color signified the formation of gold colloids in the solution. Into this seed solution was then added 5 mL of an aqueous solution containing 0.5 mmol of ascorbic acid and 0.625 mmol of NaOH, followed by the slow addition of 10 mL of a 10 mM $AgNO_3$ (0.1 mmol) solution over the course of 2 h.[25] The color of the solution was found to change from red to orange and finally to brown, due to the formation of Au@Ag core–shell nanoparticles. To cap the resulting nanoparticles with 1-dodecanethiol, in a typical experiment, 3 mL of the as-prepared core–shell nanoparticle solution was placed in a glass vial, into which was added 50 μL of HOAc. 1 mL of a $CHCl_3$ solution containing 50 μL of 1-dodecanethiol was then added to the vial and the vial was shaken for about 3 min, and the nanoparticles were found to transfer to the $CHCl_3$ phase.[26] The organic phase was collected and dried by rotary evaporation and the obtained solids were rinsed with a copious amount of methanol to remove excess thiol ligands, affording purified 1-dodecanethiol-capped Au@Ag core–shell nanoparticles.

1-Dodecanethiol-capped Ag@Au core–shell nanoparticles were prepared in a similar fashion except that silver colloids were first prepared and used as seed particles onto which a gold shell was grown from $HAuCl_4$. The presence of NaOH (solution pH > 10.8) inhibited the galvanic replacement of Ag colloids by Au(III) and facilitated the deposition of a gold shell onto the Ag surface, leading to the formation of Ag@Au core–shell nanoparticles.[27]

Preparation of Au@Ag semishell Janus nanoparticles

Au@Ag semishell Janus nanoparticles were prepared by etching off part of the silver shell from the Au@Ag core–shell nanoparticles using a H_2O_2 + NH_3 (1 : 1 mole ratio) water solution.[23,28] In brief, the monolayer of 1-dodecanethiol-capped Au@Ag core–shell nanoparticles prepared above was deposited onto the water surface of a Langmuir–Blodgett trough (NIMA Technology, model 611D). The particle monolayer was then compressed to a desired surface pressure where the interparticle edge-to-edge separation was maintained at a value smaller than twice the extended ligand chain length such that the interfacial mobility of the particles was impeded. At this point, a calculated amount of the H_2O_2 + NH_3 aqueous solution was injected into the water subphase by a Hamilton microliter syringe, where the silver shells in direct contact with water were etched away, leading to the formation of Au@Ag semi-shell Janus nanoparticles. The nanoparticles were then collected for further characterization.

Structural characterization

UV-vis absorption spectra were collected with a PerkinElmer Lambda 35 spectrometer using a 1 cm quartz cuvette. X-ray photoelectron spectra (XPS) were recorded with a PHI 5400/XPS instrument equipped with an Al K_α source operated at 350 W and 10^{-9} Torr. The morphology and sizes of the nanoparticles were characterized by transmission electron microscopy (TEM, Philips CM200 at 200 kV) studies. At least 100 nanoparticles were measured to obtain a size distribution. For inductively coupled plasma mass spectrometry (ICP-MS, PerkinElmer Optima 4300DV) measurements, about 25 μg of the nanoparticles prepared above were dissolved in 1 mL of freshly made aqua regia. The solution was then diluted by

nanopure water to 15 mL. Standard solutions of metal ions were made at a concentration of 0.5 μg mL^{-1} Ag^{+} and 1.0 μg mL^{-1} Au^{3+} with aqua regia of the same concentration.

Electrochemistry

Electrochemical studies were carried out in a standard three-electrode cell connected to a CHI-710 electrochemical workstation, with a Pt foil counter electrode and a reversible hydrogen electrode (RHE) at room temperature (25 °C). The working electrode was a rotating ring-disk electrode (RRDE, with a glassy carbon disk and a gold ring). In a typical measurement, 1 mg of the nanoparticles prepared above, 4 mg of carbon powders, and 10 μL of a Nafion solution were ultrasonically mixed in 1 mL of toluene. Then 10 μL of this solution was dropcast onto the glassy-carbon disk (5.61 mm diameter, from Pine Instruments) with a Hamilton microliter syringe. As soon as the electrode was dried, a dilute Nafion solution (0.1 wt%, 3 μL) was added onto it, and the electrode was immersed into electrolyte solutions for voltammetric measurements. The metal loadings on the electrode were all 10 μg.

Results and discussion

As mentioned above, Au@Ag semishell Janus nanoparticles were prepared by taking advantage of the selective etching of silver by H_2O_2 + NH_3 using Au@Ag core–shell nanoparticles as the starting materials.[23,28] The structures of the nanoparticles were first examined by TEM measurements. From panels (A)–(C) in Fig. 1, one can see that the Au@Ag core–shell nanoparticles were dispersed very well without apparent agglomeration, suggesting sufficient stabilization of the nanoparticles by the 1-dodecanethiol ligands. The formation of a core–shell structure in the metal cores can be clearly seen in the out-of-focus image in panel (A), as well as in the high-resolution image in panel (C) where the dark-contrast gold cores are encapsulated by a low-contrast Ag shell. From panel (C), one can also see that the nanoparticles exhibited well-defined lattice fringes with an interplanar spacing of 0.232 nm that was consistent with the (111) crystalline planes of both fcc Ag (PDF card #4-783) and gold (PDF card #4-784). After chemical etching at the air/water interface by H_2O_2 + NH_3, marked differences can be seen. From panel (D), it can be seen that whereas the majority of the nanoparticles remained well separated, a fraction of the nanoparticles aggregated into worm-like structures. This is likely due to destabilization of the nanoparticles caused by interfacial etching. In addition, the resulting nanoparticles became structurally asymmetrical with part of the Ag shells removed and part of the gold cores exposed, as manifested in panel (E), forming Au core@Ag semishell Janus nanoparticles (Scheme 1). Furthermore, statistical analysis based on more than 100 nanoparticles shows that the average

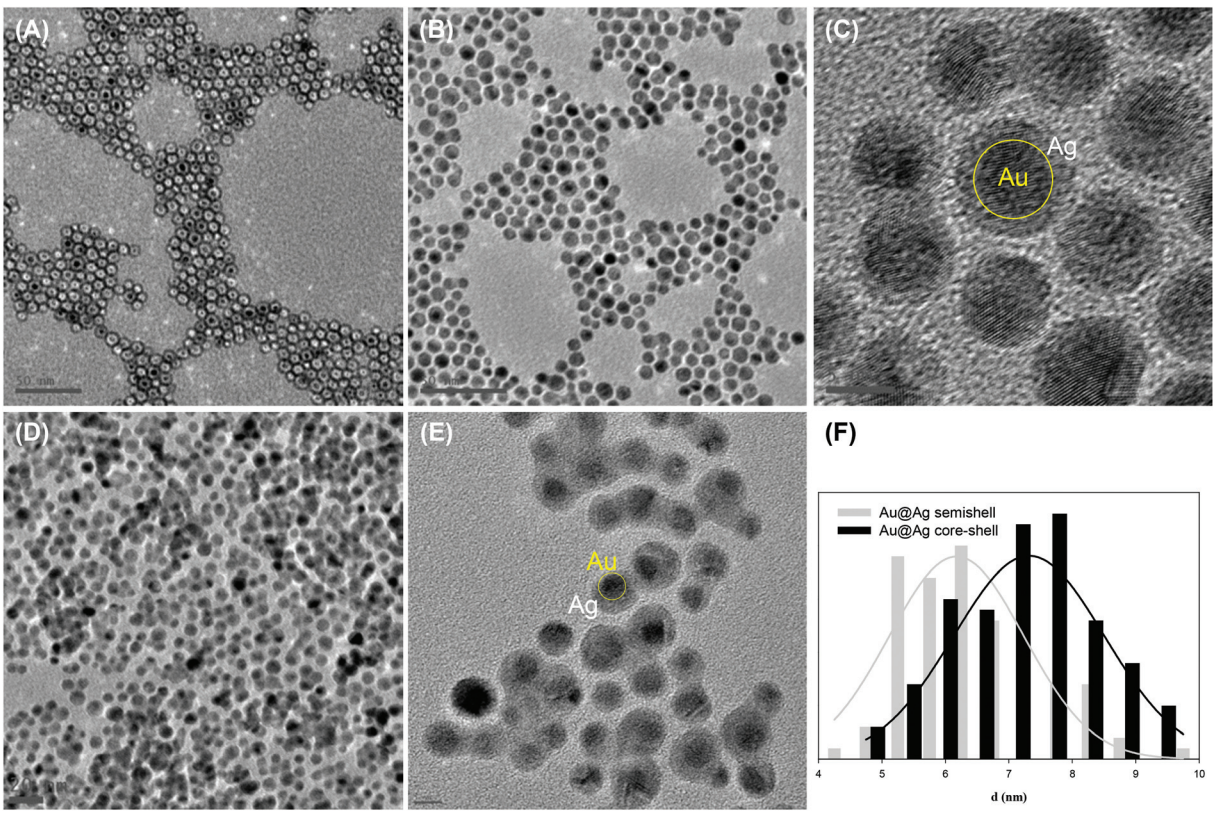

Fig. 1 Representative TEM micrographs of (A)–(C) Au@Ag core–shell nanoparticles, and (D)–(E) Au@Ag semishell nanoparticles. Scale bars are 50 nm in (A) and (B), 5 nm in (C), 20 nm in (D) and 5 nm in (E). Panel (F) is the particle size histograms of the Au@Ag core–shell and semishell nanoparticles.

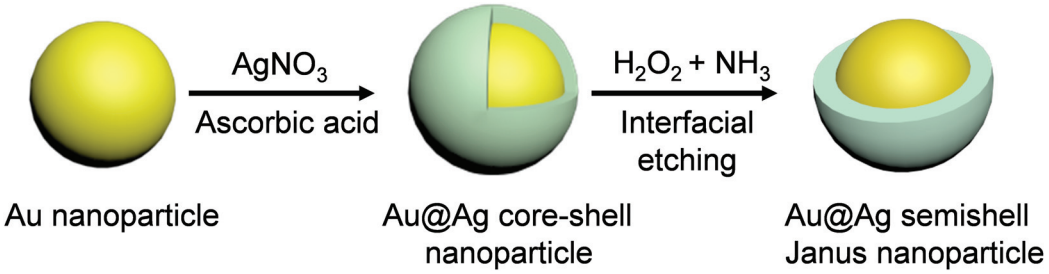

Scheme 1

size of the original Au@Ag core–shell nanoparticles is 7.3 ± 1.1 nm in diameter, with a Au core of *ca.* 5.0 nm diameter and a Ag shell of 1.1 nm in thickness (panel (C)). However, after interfacial etching by H_2O_2 + NH_3, the average diameter of the resulting semishell nanoparticles diminished to 6.4 ± 1.0 nm in diameter, as depicted in the core-size histograms in panel (F). Notably, the decrease of the nanoparticle core diameter (0.9 nm) is very close to the thickness of the Ag shell (1.1. nm). Furthermore, visual inspection showed that the majority (*ca.* 76%) of the as-produced Au@Ag core–shell nanoparticles exhibited a symmetrical contrast of the electron density (between Au and Ag), with an asymmetrical minority (24%). Yet after interfacial etching, the fraction of symmetrical nanoparticles diminished to 46% whereas the asymmetrical fraction increased markedly to 54% (Fig. S1†). These observations are in good agreement with the formation of Au core@Ag semishell Janus nanoparticles (Scheme 1).

With such a structural evolution, the corresponding nanoparticles exhibit a clear variation of the optical properties. From Fig. 2, one can see that the gold colloids (black curve) exhibit a prominent absorption peak at *ca.* 515 nm, due to the well-known surface plasmon resonance, in contrast to that of Ag nanoparticles (red curve) which appeared at around 394 nm.[29] For the Au@Ag core–shell nanoparticles (green curve), the absorption peak became broadened and centered at 440 nm, intermediate between those for Au and Ag nanoparticles;[25,30–33] After interfacial etching forming Au@Ag semishell Janus nanoparticles (blue curve), the center of the absorption peak red-shifted somewhat to 456 nm, most probably because of the exposure of part of the gold cores. In contrast, when the chemical etching was carried out with the Au@Ag core–shell nanoparticles mixed with the etchants (H_2O_2 + NH_3) in the same solvents (denoted as "bulk etching" in Fig. 2, magenta curve), the resulting nanoparticles showed an absorption maximum at *ca.* 504 nm, very close to that of the Au nanoparticles, indicating almost complete removal of the silver shell from the original Au@Ag nanoparticles.

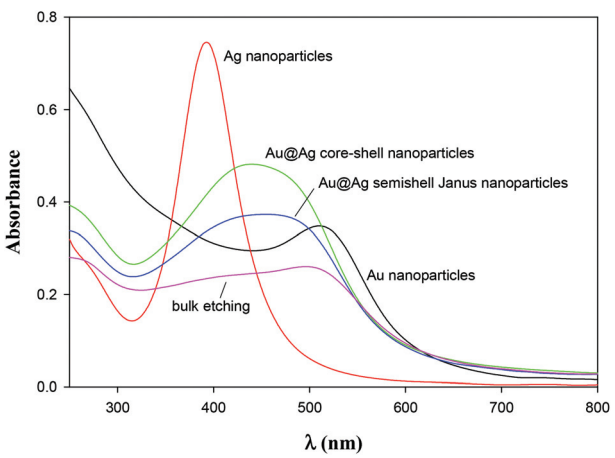

Fig. 2 UV-vis spectra of Au (black curve), Ag (red curve), Au@Ag core–shell nanoparticles (green curve), and Au@Ag Janus nanoparticles (blue curve). The spectrum of Au@Ag core–shell nanoparticles undergoing bulk etching is also included (magenta curve).

Consistent results were obtained in XPS measurements where the elemental compositions of the nanoparticles were quantified. Fig. 3 depicts the high-resolution scans of the (top panel) Ag 3d and (bottom panel) Au 4f electrons of the Au@Ag core–shell and semishell Janus nanoparticles. It can be seen that the original Au@Ag core–shell nanoparticles exhibited a doublet at 368.0 and 374.0 eV, corresponding to the $3d_{5/2}$ and $3d_{3/2}$ electrons of metallic silver,[34,35] whereas the doublet for the Au 4f electrons appears at 83.4 eV and 87.1 eV, consistent with those of metallic gold.[36] For the semishell Janus nanoparticles, the binding energies are somewhat higher, at 368.4 and 374.5 eV for Ag 3d and 83.9 and 87.4 eV for Au 4f. It has been known that the binding energy of the Ag 3d electrons decreases as the oxidation state increases. For instance, Hoflund and Hazos observed a decrement of about 0.3 eV from metallic Ag to Ag_2O and then to AgO.[37] Ibele *et al.* also observed a red-shift of *ca.* 0.4 eV of the Ag 3d binding energy when Au–Ag–Au trisegment nanorods were treated with H_2O_2, due to the formation of Ag_2O.[38] In the present study, the fact that semishell Janus nanoparticles exhibited higher binding energies (by *ca.* 0.4 eV) of the Ag 3d electrons than the original Au@Ag core–shell nanoparticles suggested enhanced charge compensation from Au to Ag,[39] as partial removal of the Ag shell (*i.e.*, higher Au : Ag atomic ratio) meant that silver oxide on the nanoparticle surface would be more likely to be reduced by electrons contributed from Au, and the reduced oxidation state led to a higher binding energy of the Ag 3d electrons. Such a charge compensation mechanism may also account for the increase of the binding energy of the Au 4f electrons, with additional contributions likely arising from direct adsorption of thiol ligands on the Au surface upon removal of part of the Ag shell.[40]

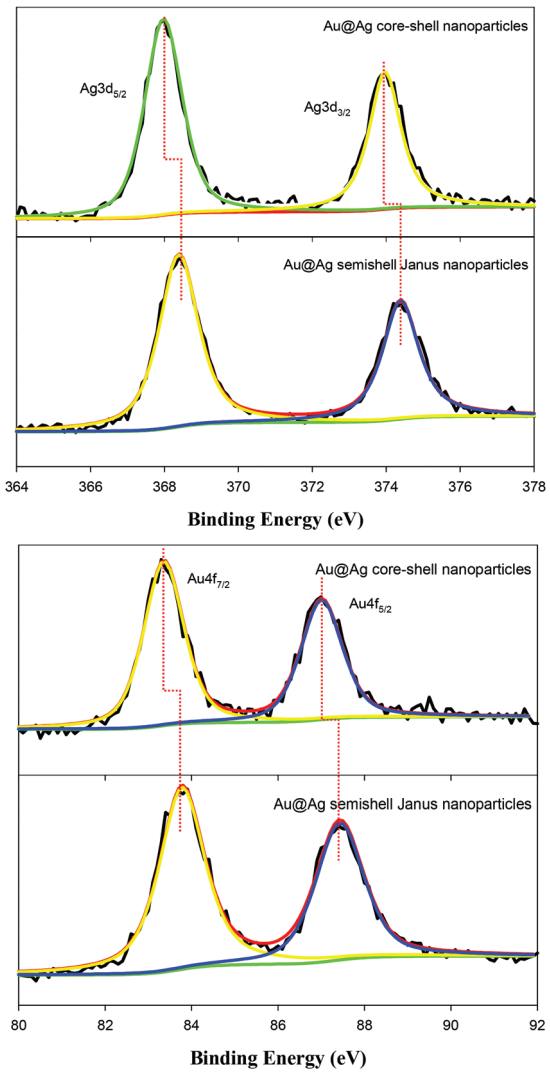

Fig. 3 XPS spectra of (top) Ag 3d and (bottom) Au 4f electrons of Au@Ag core–shell and semishell Janus nanoparticles. Black curves are experimental data and colored curves are deconvolution fits.

Furthermore, based on the integrated peak areas of the Ag 3d and Au 4f electrons, the Ag : Au atomic ratio was estimated to be 2.36 : 1 for the Au@Ag core–shell nanoparticles, which is consistent with the nanoparticle structures that consisted of a gold core of *ca.* 5.0 nm in diameter and a Ag shell of 1.1 nm in thickness, as suggested in TEM measurements (Fig. 1); and the Ag : Au atomic ratio decreased to only 1.25 : 1 for the Au@Ag semishell Janus nanoparticles. Consistent results were obtained in ICP-MS measurements, where the Ag : Au atomic ratio was estimated to be 2.53 : 1 for the Au@Ag core–shell nanoparticles, but only 1.41 : 1 for the semishell Janus nanoparticles. In both measurements, the fact that the nanoparticles lost about 50% of the Ag content suggests that indeed almost half of the Ag shell was removed by interfacial etching.

Note that consistent results were also obtained of the binding energies of the Ag 3d and Au 4f electrons for the Ag@Au core–shell nanoparticles (Fig. S2†), where the Ag : Au atomic ratio was found to be very close at 1.61 : 1. This indicates that the Ag@Au core–shell nanoparticles and Au@Ag semishell Janus nanoparticles may be approximated as structural isomers. Yet, their electrocatalytic activity towards ORR was markedly different, as shown below.

Experimentally, the nanoparticles prepared above were first loaded onto the glassy carbon disk of a rotating ring-disk electrode and subject to repeated potential cycling within the range of +0.1 V to +1.1 V in a nitrogen saturated 0.1 M NaOH solution until a steady voltammogram appeared. The electrocatalytic activity tests were then carried out in the same solution but saturated with oxygen. Fig. 4(A) depicts the RDE voltammograms of a glassy carbon electrode modified with Au@Ag core–shell and semishell Janus nanoparticles, as well as Ag@Au core–shell nanoparticles (Fig. S3†) at the same loading of 10 μg. It can be seen that for the Au@Ag Janus nanoparticles, nonzero cathodic currents started to emerge at about +0.95 V (*vs.* RHE) and the currents reached a plateau at around +0.60 V. This performance is markedly better than that of the Au@Ag core–shell nanoparticles where the onset potential was 40 mV less positive at +0.91 V; whereas the Ag@Au core–shell nanoparticles displayed the least positive onset potential at +0.77 V. The diffusion-limited current also decreases in the same order. For instance, at +0.40 V, the current density was 92 A g^{-1} for Au@Ag semishell Janus nanoparticles, 80 A g^{-1} for Au@Ag core–shell nanoparticles, and only 40 A g^{-1} for Ag@Au core–shell nanoparticles. Altogether, these results indicate that a silver shell is more active in catalyzing ORR than a gold one, and the activity was even higher with a silver half-shell where both Ag and Au surfaces were accessible (note that Ag@Au semishell nanoparticles could not be produced as Au was chemically inert against H_2O_2 and NH_3, Fig. S4†).

Panel (B) depicts the RRDE voltammograms of the Au@Ag semishell Janus nanoparticles at different electrode rotation rates (from 100 to 2500 rpm). One can see that the voltammetric currents increased with the increasing electrode rotation rate and the disk currents were at least two orders of magnitude higher than those at the ring electrode, suggesting that only a minimal amount of peroxide intermediates was produced during ORR. In fact, the number of electron transfers involved in the reduction of one O_2 molecule on the nanoparticles was determined by $n = 4I_D/(I_D + I_R/N)$, where I_D and I_R are disk and ring currents, respectively. By using the disk and ring currents collected at 1600 rpm as an example (RRDE voltammograms for Au@Ag and Ag@Au core–shell nanoparticles are included in Fig. S5†), one can see that within the wide potential range of +0.90 V to +0.10 V, the n values increased markedly in the order of Ag@Au core shell < Au@Ag core–shell < Au@Ag semishell nanoparticles, as evidenced in panel (C). For instance, at +0.60 V, the Au@Ag semishell Janus nanoparticles exhibited the highest n value of 3.98, somewhat higher than that (3.92) of Au@Ag core–shell nanoparticles, while Ag@Au core–shell nanoparticles showed the lowest n value of 3.53, corresponding to a peroxide yield of 1%, 4% and 23.5%, respectively. This means that oxygen mostly underwent

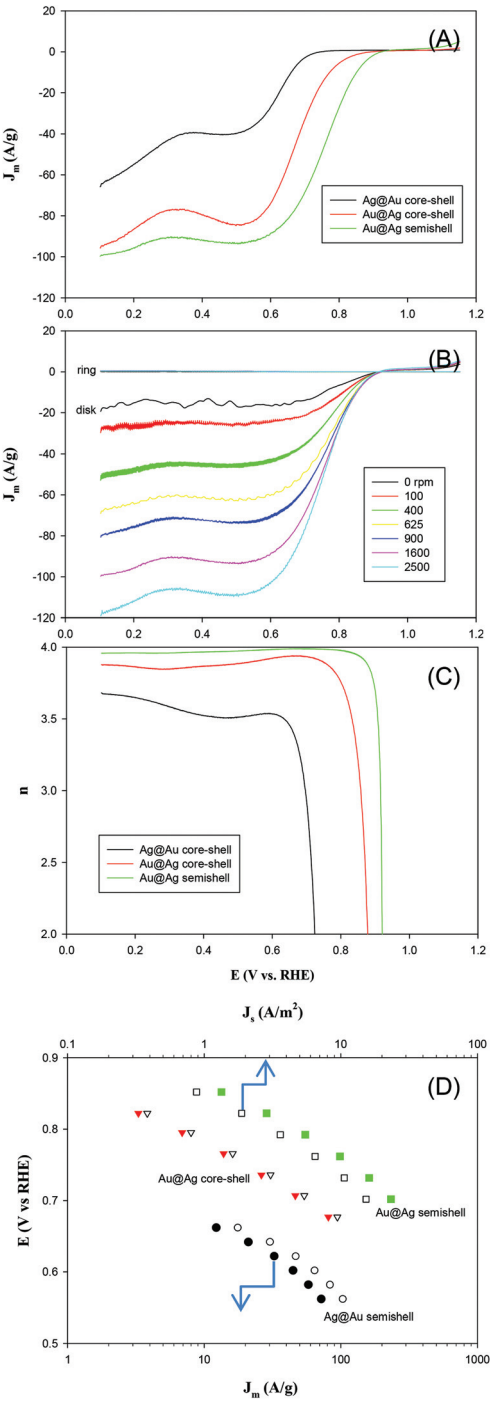

Fig. 4 (A) ORR polarization curves at 1600 rpm for Ag@Au (black curve), Au@Ag (red curve) core–shell nanoparticles and Au@Ag Janus nanoparticles (green curve). (B) RRDE voltammograms of a glassy carbon electron modified with the Au@Ag Janus nanoparticles in oxygen-saturated 0.1 M NaOH at varied rotation rates (specified in figure legends). (C) Variation of the number of electron transfers (*n*) with electrode potentials for Ag@Au (black curve), Au@Ag (red curve) core–shell nanoparticles and Au@Ag Janus nanoparticles (green curve). Data were obtained by using the respective RRDE voltammograms at 1600 rpm. (D) Tafel plots derived from panel (B) where solid symbols are the mass activity (J_m) and empty symbols are specific activity (J_s). The loading of metal nanoparticle catalysts was all 10 μg. The disk potential ramp was 10 mV s^{-1} and the ring potential was set at +1.5 V.

four-electron reduction at Au@Ag semishell Janus and core–shell nanoparticles, $O_2 + 2H_2O + 4e \rightarrow 4OH$, whereas a rather significant amount of peroxide species was generated during ORR on Ag@Au core–shell nanoparticles. Note that the results were highly reproducible and repeated measurements showed no more than 10% deviation.

The clear discrepancy of the ORR activity among these three nanoparticle catalysts may be understood within the context of surface accessibility for oxygen adsorption and reduction. Note that for bimetallic core–shell nanoparticles, the electrocatalytic activity is mainly determined by the shell materials. Prior studies have shown that a Ag surface displays better ORR catalytic activity than a gold one because of its stronger oxygen binding energy.[41–43] The ORR activity was further enhanced when both Ag and Au surfaces were exposed and accessible, likely due to synergistic interactions between the two metals (*vide infra*).

Similar behaviors can be observed with the mass-specific kinetic current density (J_m), as depicted in the Tafel plot of panel (D). It can be seen that the J_m increased with an increasingly negative electrode potential. In addition, the activity of the Janus nanoparticles is significantly higher than that of the core–shell nanoparticles. For instance, at +0.66 V, J_m for Au@Ag semishell Janus nanoparticles was estimated to be 633 A g^{-1}, about 4.8 times that (131 A g^{-1}) of Au@Ag core–shell nanoparticles and 45 times that (14 A g^{-1}) of Ag@Au core–shell nanoparticles. Consistent results can also be seen in the comparison of the corresponding specific activity (J_s, which was estimated by normalizing the kinetic currents against the electrochemical surface area quantified by Pb UPD, Fig. S6†). For instance, at +0.66 V, J_s for Au@Ag semishell Janus nanoparticles was *ca.* 23.0 A m^{-2}, about 2.2 times that (10.5 A m^{-2}) of Au@Ag core–shell nanoparticles and 13 times that (1.78 A m^{-2}) of Ag@Au core–shell nanoparticles.

Note that for oxygen electroreduction at nanoparticle catalyst surfaces, the Tafel slopes are typically found at 60 or 120 mV dec^{-1}, where the former corresponds to a pseudo two-electron reaction as the rate determining step and in the latter, the rate determining step is the first-electron reduction of oxygen.[44] In the present study, linear regressions show that the slopes are 128 mV dec^{-1}, 104 mV dec^{-1} and 119 mV dec^{-1} for Ag@Au core–shell, Au@Ag core–shell nanoparticles and Au@Ag semishell Janus nanoparticles, respectively, suggesting that ORR on these three nanoparticle catalysts was all likely limited by the first electron reduction. Such behaviors have been observed on the Pt or Pt alloy surface, suggesting that the catalytic mechanism of ORR on AgAu resembles that on Pt, which involves O–O bond breaking and adsorption of oxygenate intermediates, but is distinctly different from that on pure Ag or Au catalysts, where the ORR rate is limited by the absorption of O_2 molecules on the metal surface and the first electron transfer.[45–47]

Notably, within the context of onset potential, *n* value, and mass/specific activity, the electrocatalytic performance of the Au@Ag semishell Janus nanoparticles prepared above is markedly better than those observed with monometallic Au or Ag

nanoparticles of similar sizes,[43,48,49] and even comparable to that of commercial Pt/C catalysts (except with a lower mass activity).[50] In addition, in comparison with the AuAg alloy nanoparticles reported in recent literature, the ORR activity of the semishell Janus nanoparticles is also enhanced. For instance, the onset potential for ORR observed above for the Au@Ag semishell Janus nanoparticles was at least 30 mV more positive than those for the Au@Ag bimetallic Janus nanoparticles prepared by interfacial galvanic exchange reactions[18] as well as for AgAu (bulk) alloy nanoparticles.[51,52]

It is most likely that the improved performance of the Au@Ag Janus nanoparticles over Au@Ag or Ag@Au core–shell nanoparticles is due to the partial exposure of the core metal surface to oxygen absorption. As mentioned earlier, for core–shell nanoparticles, the catalytic activity is mainly dictated by the shell materials, as the inner cores are inaccessible[21] but may impact the catalytic activity through surface strain, particle size and shape.[20] In the present study, these contributions are likely to be minimal as Ag and Au exhibit almost no lattice mismatch and the three nanoparticles were largely of the same size and shape (Fig. 1 and S3†).[53] Instead, the remarkable ORR performance observed with the Au@Ag semishell nanoparticles may be ascribed to the enhanced charge transfer from Au to Ag,[39] as manifested in XPS measurements (Fig. 3), which inhibited the formation of (inactive) silver oxide under ORR conditions in alkaline media. This resulted in a more reactive Ag surface for ORR than pure Ag,[54–56] as reflected by a positive shift of the equilibrium potential for the first electron transfer reaction and a reduced overpotential and positive shift of the onset potential.[51]

Conclusion

In the present study, gold core@Ag semishell Janus nanoparticles were prepared, for the first time ever, by interfacial etching of Au@Ag core–shell nanoparticles on the water surface based on the Langmuir method. The asymmetrical nanoparticle structures were confirmed by TEM, XPS and UV-vis absorption measurements. The resulting bimetallic Janus nanoparticles exhibited markedly enhanced electrocatalytic activity in oxygen reduction, as compared to their Au@Ag and Ag@Au core–shell counterparts, within the context of onset potential, number of electron transfers, and kinetic current density. This was likely due to partial charge transfer from Au to Ag that optimized oxygen adsorption on the metal surfaces. These results further demonstrate the significance of the interfacial engineering in nanoparticle modification and the impact on their electrocatalytic activity.

Acknowledgements

This work was supported in part by the National Science Foundation (CHE-1265635 and DMR-1409396). TEM and XPS work was carried out at the National Center for Electron Microscopy and the Molecular Foundry at the Lawrence Berkeley National Laboratory, which is supported by the US Department of Energy, as part of a user project.

References

1 X. Qin, A. Xu, L. Liu, W. Deng, C. Chen, Y. Tan, Y. Fu, Q. Xie and S. Yao, *Chem. Commun.*, 2015, **51**, 8540–8543.
2 D. Bodhisatwa, F. Fernandez, A. John and C. P. Sharma, *J. Biomater. Tissue Eng.*, 2012, **2**, 299–306.
3 P. D. Howes, R. Chandrawati and M. M. Stevens, *Science*, 2014, **346**, 1247390.
4 L. H. Guo, Y. Xu, A. R. Ferhan, G. N. Chen and D. H. Kim, *J. Am. Chem. Soc.*, 2013, **135**, 12338–12345.
5 S. J. Guo, X. Zhang, W. L. Zhu, K. He, D. Su, A. Mendoza-Garcia, S. F. Ho, G. Lu and S. H. Sun, *J. Am. Chem. Soc.*, 2014, **136**, 15026–15033.
6 A. Walther and A. H. Muller, *Chem. Rev.*, 2013, **113**, 5194–5261.
7 A. Perro, S. Reculusa, S. Ravaine, E. B. Bourgeat-Lami and E. Duguet, *J. Mater. Chem.*, 2005, **15**, 3745–3760.
8 M. Lattuada and T. A. Hatton, *Nano Today*, 2011, **6**, 286–308.
9 Y. Song and S. W. Chen, *Chem. – Asian J.*, 2014, **9**, 418–430.
10 J. B. Lassiter, J. Aizpurua, L. I. Hernandez, D. W. Brandl, I. Romero, S. Lal, J. H. Hafner, P. Nordlander and N. J. Halas, *Nano Lett.*, 2008, **8**, 1212–1218.
11 H. Yu, M. Chen, P. M. Rice, S. X. Wang, R. L. White and S. H. Sun, *Nano Lett.*, 2005, **5**, 379–382.
12 S. Pradhan, D. Ghosh and S. W. Chen, *ACS Appl. Mater. Interfaces*, 2009, **1**, 2060–2065.
13 T. Chen, G. Chen, S. X. Xing, T. Wu and H. Y. Chen, *Chem. Mater.*, 2010, **22**, 3826–3828.
14 J. Zeng, C. Zhu, J. Tao, M. S. Jin, H. Zhang, Z. Y. Li, Y. M. Zhu and Y. N. Xia, *Angew. Chem., Int. Ed.*, 2012, **51**, 2354–2358.
15 X. Guo, Q. Zhang, Y. H. Sun, Q. Zhao and J. Yang, *ACS Nano*, 2012, **6**, 1165–1175.
16 A. J. Logsdail and R. L. Johnston, *J. Phys. Chem. C*, 2012, **116**, 23616–23628.
17 X. M. Lu, H. Y. Tuan, J. Y. Chen, Z. Y. Li, B. A. Korgel and Y. N. Xia, *J. Am. Chem. Soc.*, 2007, **129**, 1733–1742.
18 Y. Song, K. Liu and S. W. Chen, *Langmuir*, 2012, **28**, 17143–17152.
19 C. Zhu, J. Zeng, J. Tao, M. C. Johnson, I. Schmidt-Krey, L. Blubaugh, Y. M. Zhu, Z. Z. Gu and Y. N. Xia, *J. Am. Chem. Soc.*, 2012, **134**, 15822–15831.
20 X. Zhang and G. Lu, *J. Phys. Chem. Lett.*, 2014, **5**, 292–297.
21 X. W. Liu, D. S. Wang and Y. D. Li, *Nano Today*, 2012, **7**, 448–466.
22 G. X. Wang, H. M. Wu, D. Wexler, H. K. Liu and O. Savadogo, *J. Alloys Compd.*, 2010, **503**, L1–L4.
23 Y. Song and S. W. Chen, *Nanoscale*, 2013, **5**, 7284–7289.
24 N. S. Ieong, K. Brebis, L. E. Daniel, R. K. O'Reilly and M. I. Gibson, *Chem. Commun.*, 2011, **47**, 11627–11629.

25 A. K. Samal, L. Polavarapu, S. Rodal-Cedeira, L. M. Liz-Marzan, J. Perez-Juste and I. Pastoriza-Santos, *Langmuir*, 2013, **29**, 15076–15082.
26 M. Lista, D. Z. Liu and P. Mulvaney, *Langmuir*, 2014, **30**, 1932–1938.
27 Y. Yang, J. Y. Liu, Z. W. Fu and D. Qin, *J. Am. Chem. Soc.*, 2014, **136**, 8153–8156.
28 M. M. Shahjamali, M. Bosman, S. W. Cao, X. Huang, X. H. Cao, H. Zhang, S. S. Pramana and C. Xue, *Small*, 2013, **9**, 2880–2886.
29 J. A. Creighton and D. G. Eadon, *J. Chem. Soc., Faraday Trans.*, 1991, **87**, 3881–3891.
30 B. Rodriguez-Gonzalez, A. Burrows, M. Watanabe, C. J. Kiely and L. M. Liz-Marzan, *J. Mater. Chem.*, 2005, **15**, 1755–1759.
31 S. K. Cha, J. H. Mun, T. Chang, S. Y. Kim, J. Y. Kim, H. M. Jin, J. Y. Lee, J. Shin, K. H. Kim and S. O. Kim, *ACS Nano*, 2015, **9**, 5536–5543.
32 Y. Ma, W. Li, E. C. Cho, Z. Li, T. Yu, J. Zeng, Z. Xie and Y. Xia, *ACS Nano*, 2010, **4**, 6725–6734.
33 S. Underwood and P. Mulvaney, *Langmuir*, 1994, **10**, 3427–3430.
34 S. W. Han, Y. Kim and K. Kim, *J. Colloid Interface Sci.*, 1998, **208**, 272–278.
35 A. Q. Wang, C. M. Chang and C. Y. Mou, *J. Phys. Chem. B*, 2005, **109**, 18860–18867.
36 C. W. Yi, K. Luo, T. Wei and D. W. Goodman, *J. Phys. Chem. B*, 2005, **109**, 18535–18540.
37 G. B. Hoflund, Z. F. Hazos and G. N. Salaita, *Phys. Rev. B: Condens. Matter*, 2000, **62**, 11126–11133.
38 M. E. Ibele, R. Liu, K. Beiswenger and A. Sen, *J. Mater. Chem.*, 2011, **21**, 14410–14413.
39 D. M. Mott, T. N. A. Dao, P. Singh, C. Shankar and S. Maenosono, *Adv. Colloid Interface Sci.*, 2012, **185**, 14–33.
40 M. J. Hostetler, J. E. Wingate, C. J. Zhong, J. E. Harris, R. W. Vachet, M. R. Clark, J. D. Londono, S. J. Green, J. J. Stokes, G. D. Wignall, G. L. Glish, M. D. Porter, N. D. Evans and R. W. Murray, *Langmuir*, 1998, **14**, 17–30.
41 J. K. Norskov, J. Rossmeisl, A. Logadottir, L. Lindqvist, J. R. Kitchin, T. Bligaard and H. Jonsson, *J. Phys. Chem. B*, 2004, **108**, 17886–17892.
42 S. Siahrostami, A. Verdaguer-Casadevall, M. Karamad, D. Deiana, P. Malacrida, B. Wickman, M. Escudero-Escribano, E. A. Paoli, R. Frydendal, T. W. Hansen, I. Chorkendorff, I. E. L. Stephens and J. Rossmeisl, *Nat. Mater.*, 2013, **12**, 1137–1143.
43 P. Singh and D. A. Buttry, *J. Phys. Chem. C*, 2012, **116**, 10656–10663.
44 I. A. Pasti, N. M. Gavrilov and S. V. Mentus, *Int. J. Electrochem. Sci.*, 2012, **7**, 11076–11090.
45 N. M. Markovic, H. A. Gasteiger and N. Philip, *J. Phys. Chem.*, 1996, **100**, 6715–6721.
46 V. R. Stamenkovic, B. S. Mun, M. Arenz, K. J. Mayrhofer, C. A. Lucas, G. Wang, P. N. Ross and N. M. Markovic, *Nat. Mater.*, 2007, **6**, 241–247.
47 D. Mei, Z. D. He, Y. L. Zheng, D. C. Jiang and Y. X. Chen, *Phys. Chem. Chem. Phys.*, 2014, **16**, 13762–13773.
48 F. Mirkhalaf and D. J. Schiffrin, *Langmuir*, 2010, **26**, 14995–15001.
49 L. Tammeveski, H. Erikson, A. Sarapuu, J. Kozlova, P. Ritslaid, V. Sammelselg and K. Tammeveski, *Electrochem. Commun.*, 2012, **20**, 15–18.
50 L. Genies, R. Faure and R. Durand, *Electrochim. Acta*, 1998, **44**, 1317–1327.
51 P. Hu, Y. Song, L. Chen and S. Chen, *Nanoscale*, 2015, **7**, 9627–9636.
52 C. X. Yang, B. Huang, L. Xiao, Z. D. Ren, Z. L. Liu, J. T. Lu and L. Zhuang, *Chem. Commun.*, 2013, **49**, 11023–11025.
53 J. F. Sanchez-Ramirez, U. Pal, L. Nolasco-Hernandez, J. Mendoza-Alvarez and J. A. Pescador-Rojas, *Nanomaterials*, 2008, 620412.
54 T. Van Cleve, E. Gibara and S. Linic, *ChemCatChem*, 2016, **8**, 256–261.
55 G. Q. He, Y. Song, B. Phebus, K. Liu, C. P. Deming, P. G. Hu and S. W. Chen, *Sci. Adv. Mater.*, 2013, **5**, 1727–1736.
56 G. Mills, M. S. Gordon and H. Metiu, *J. Chem. Phys.*, 2003, **118**, 4198–4205.

